Transmembrane voltage analyses in spheroidal cells in response to an intense ultrashort electrical pulse

Q. Hu
Department of Engineering and Technology, Central Michigan University, Mt Pleasant, Michigan 48859, USA

R. P. Joshi
Department of Electrical and Computer Engineering, Old Dominion University, Norfolk, Virginia 23529-0246, USA

(Received 12 August 2008; revised manuscript received 9 October 2008; published 7 January 2009)

Self-consistent evaluations of both the transmembrane potential (TMP) and possible electroporation density across membrane of spheroidal cells in response to ultrashort, high-intensity pulses are reported and discussed. Most treatments in the literature have been based on spherical cells, and this represents a step towards more realistic analyses. The present study couples the Laplace equation with Smoluchowski theory of pore formation, to yield dynamic membrane conductivities that influence the TMP. It is shown that the TMP induced by pulsed external voltages can be substantial higher in oblate spheroids as compared to spherical or prolate spheroidal cells. Flattening of the surface area in oblate spheroids leads to both higher electric fields seen by the membrane, and allows a great fraction of the surface area to be porated. This suggests that biomedical applications such as drug delivery and electrochemotherapy could work best for flatter-shaped cells, and secondary field-enabled orienting would be beneficial. Results for arbitrary field orientations and different cell sizes have also been presented.

DOI: 10.1103/PhysRevE.79.011901 PACS number(s): 87.50.−a, 87.16.A−, 87.17.Aa

I. INTRODUCTION

A large body of literature has now begun to emerge on the application of electric pulses for biomedical engineering. Potential uses include cellular response manipulation, cell hybridization in the formation of monoclonal antibodies, electrically assisted drug delivery, bacterial decontamination, the production of hybridomas, injection of xenomolecules such as hormones, proteins, RNA, DNA, and chromosomes, and electrofusion of dielectrophoretically aligned cells [1–17]. Generally, the underlying principle used in these techniques is cellular electroporation. This phenomena, first reported several decades ago [18,19] involves the structural rearrangement of the lipid bilayer molecules that constitute the cell membrane. As a result, aqueous pathways are created that effectively lead to orders-of-magnitude enhancements in the permeability and transport of ions and molecules through the plasma membrane. This process facilitates the entry of drug molecules into cells and leads to applications such as electrochemotherapy and electrogene therapy [6,8,9,20,21]. The dimension and distribution of the membrane electropores so formed typically depend on both the magnitude and pulse durations of the applied electric fields. At this time the biophysics of electroporation is somewhat understood based on both continuum and molecular-level analyses [22–30], though some open issues remain [31]. Experiments including those based on fluorescent dye imaging, have clearly demonstrated the increased transport of molecules upon electric pulsing [32,33]. Ionic changes as well as calcium release from the endoplasmic reticulum (and its transport through the plasma membrane) has been detected [34,35]. All of these processes collectively point to the enhanced transport and altered "conductivity" of the membranes.

A more recent development, in this context, has been the use of electric pulses with very high fields (~100 kV/cm or higher) and pulse durations in the nanosecond range [36–38]. From a practical standpoint, such high-intensity, nanosecond, pulsed electric fields (nsPEFs) have been shown to be useful as a nonthermal tool capable of modulating the response both at the plasma membrane and reaching the interior cellular organelles. Various biological applications have been demonstrated, ranging from cellular electroporation [33], electrically triggered intracellular calcium release [34,35], the nonthermal destruction of micro-organisms [33,39,40], killing of tumor cells [33,41], DNA damage [42], and temporary blockage of action potential propagation in nerves [43,44]. The hallmark of such nsPEFs is the creation of high-density nanometer-sized pores in cell membranes, including those covering the various inner-organnelles. This has been roughly been supported by tracking fluorescent dyes in flow cytometry experiments [32,33], and is also in line with analytical [45–48] and molecular dynamic calculations [49–51]. Other observed effects include conformational changes of membrane-embedded proteins and disruption of voltage-gated channels [52]. Cell death upon exposure to pulses of high-electric field (~100 kV/cm or more) intensity has also been well established experimentally [53,54].

In all of the above applications, the development of a transmembrane potential (TMP) is critical to influencing and modulating the cellular bioresponse. Membranes develop the highest voltages given their near impermeability making them behave as dielectric capacitor elements. Almost all analyses and calculations of the TMP created as the direct result of applying external pulsing have assumed spherical cells. In biology, examples of such spherical shapes are vesicles, protoplasts, murine myeloma cells [55], and some bacteria such as *Streptococcus* [56]. However, most other cells are nonspherical in nature. Hence, the reported analyses of possible bioelectric effects on spherical cells have a limited applicability and must be regarded as being somewhat

approximate at best. For nonspherical cells, the shape and orientation (e.g., the major axis with respect to the electric field direction) begin to play an important role. However, as it turns out, many cells deviating from the spherical shape do exhibit rotational symmetry and can be represented either as prolate or oblate spheroids fairly accurately. For example, mammalian red blood cells are close to an oblate spheroidal shape, while retina photoreceptor cells [57], many bacteria such as *E. coli, Pseudomonas* [56], and yeasts [58] roughly have a prolate spheroidal geometry. This makes a compelling case, at least from the practical standpoint, to examine bioelectric pulsing effects in such spheroidal cell shapes for a more realistic and accurate analyses and predictions. Hence, self-consistent calculations for spheroidal cell geometries that include time- and voltage-dependent membrane electroporation are analyzed and discussed in this contribution.

There have been only a few reports in the literature on analyses that deviate from the spherical geometry. Pucihar *et al.* [59] used a finite element approach to solve for the TMP in irregularly shaped cells, though electroporation was not explicitly considered. An earlier report by this group had considered a lattice model of spherical cells which allowed for the inclusion of identical multiple cells [60]. Analyses for multiple cells have also been considered by Gowrishankar and Weaver [61] using a distributed lattice model, and by Joshi *et al.* [62] on the basis of a Voronoi network of cells. However, in all these multicell approaches, spherical cell geometries had been used. The only other reports on spheroidal cells to our knowledge were those by Kotnik and Miklavcic [63], analyses for ac voltage signals by Maswiwat *et al.* [64,65], and a very recent report [66] by this same group. In neither case though, was electroportion considered in a self-consistent manner.

II. MODELING DETAILS

A. Time-dependent transmembrane potential calculations

Self-consistent approaches to calculating the transmembrane potential of spherical cells in response to external ultra-short pulses have been discussed in our previous papers [29,67]. Basically, the external field produces a TMP, which could lead to poreformation at the membrane. This pore density modulates the local conductivity, thereby, affecting the local fields and the subsequently development of the TMP. Here we extend that approach to time-dependent TMP calculations in spheroidal cells based on a coupled solution of the Laplace and Smoluchowski equations. The external electric field $E_o(t)$ was taken to be along the z axis, the axis of revolution, and assumed to have the exact time dependent shape as the external wave form. The schematic shown in Fig. 1(a) represents a prolate spheroidal cell suspended in a medium and Fig. 1(b) represents an oblate spheroidal cell. The geometric model is similar to that used by Jerry and Popel [68] for analyzing potentials induced by alternating fields. The cells in Fig. 1 are characterized by an outer equatorial radius a_o, an inner equatorial radius a_i, an outer polar radius b_o, and an inner polar radius b_i. It is assumed that the outer spheroid and inner spheroid share the same foci. The focal distance c of both spheroids can then be found as $c=\sqrt{b_i^2-a_i^2}=\sqrt{b_o^2-a_o^2}$

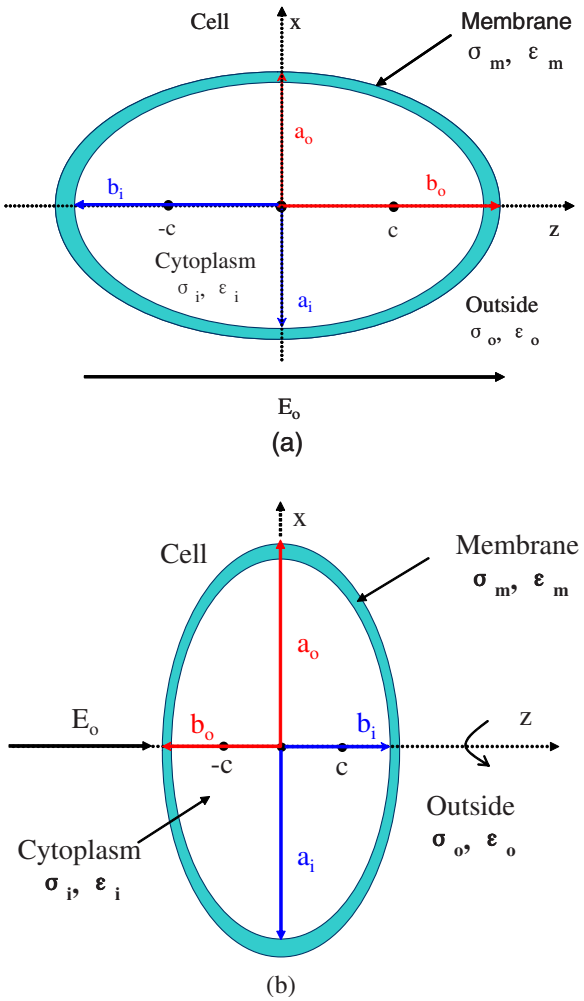

FIG. 1. (Color online) Schematic of the spheroidal cell model for the transmembrane potential calculation. (a) Prolate spheroid with $b>a$. (b) Oblate spheroid with $b<a$.

for prolate $(b_i>a_i)$ and $c=\sqrt{a_i^2-b_i^2}=\sqrt{a_o^2-b_o^2}$ for oblate $(b_i<a_i)$ spheroids, respectively. Thickness at the polar points is $h=b_o-b_i$ for the prolate and $h=a_o-a_i$ for oblate spheroids. The outer region has an assigned conductivity σ_o and permittivity ε_o, while the corresponding parameters for the cell membrane are σ_m and ε_m. In Fig. 1, σ_i and ε_i are the conductivity and permittivity of the cytoplasm.

The TMP Φ can be obtained by solving the Laplace's equation for the prolate spheroid [69]

$$\nabla^2\Phi=\frac{1}{c^2(u^2-v^2)}\left\{\frac{\partial}{\partial u}\left[(u^2-1)\frac{\partial\Phi}{\partial u}\right]+\frac{\partial}{\partial v}\left[(1-v^2)\frac{\partial\Phi}{\partial v}\right]\right\}+\frac{1}{c^2(u^2-1)(1-v^2)}\frac{\partial^2\Phi}{\partial\varphi^2}=0. \quad (1)$$

Here the usual prolate-spheroidal coordinates (u,v,φ) have been used. Coordinates u and v are orthogonal, $u\geqslant 1$, $-1\leqslant v\leqslant 1$, and $0\leqslant\varphi<2\pi$. The prolate-spheroidal coordinates (u,v,φ) are related to Cartesian coordinates by

$$x=c\sqrt{(u^2-1)(1-v^2)}\cos\varphi, \quad (2a)$$

$$y = c\sqrt{(u^2-1)(1-v^2)}\sin\varphi, \tag{2b}$$

$$z = cuv. \tag{2c}$$

Here $u=\cosh(\xi)$ and $v=\cos(\theta)$ with $\xi>0$ and $\theta\in[0,\pi]$. Since the prolate spheroid is symmetrical with regards to the angle by φ, the second term in Eq. (1) is zero and can be omitted. Hence, we obtain

$$\nabla^2\Phi = \frac{\partial}{\partial u}\left[(u^2-1)\frac{\partial\Phi}{\partial u}\right] + \frac{\partial}{\partial v}\left[(1-v^2)\frac{\partial\Phi}{\partial v}\right] = 0. \tag{3}$$

By separation of variables, Eq. (3) can be easily solved. The time-dependent solution of the Laplace's equation is

$$\phi_i(u,v,t) = A_i(t)uv, \quad u \leqslant u_i, \tag{4a}$$

$$\phi_m(u,v,t) = v\left[A_m(t)u + B_m(t)\left(\frac{u}{2}\ln\frac{u+1}{u-1} - 1\right)\right], \quad u_i < u < u_o, \tag{4b}$$

$$\phi_o(u,v,t) = v\left[-cE_o(t)u + B_o(t)\left(\frac{u}{2}\ln\frac{u+1}{u-1} - 1\right)\right], \quad u > u_o, \tag{4c}$$

where $\phi_o(u,v,t)$, $\phi_m(u,v,t)$, and $\phi_i(u,v,t)$ are the potentials at the outer region, the plasma membrane, and the cytoplasm, respectively. Here $u_i=b_i/c$, $u_o=b_o/c$, and $E_0(t)$ is the externally applied electric field. Also, $A_i(t)$, $A_m(t)$, $B_m(t)$, and $B_o(t)$ are the coefficients that can be determined by applying matching boundary conditions at the interfaces of the three regions.

Similarly, the transmembrane potential Φ for an oblate spheroidal cell can be obtained by solving the following Laplace's equation in oblate-spheroid coordinates:

$$\nabla^2\Phi = \frac{1}{c^2(u^2+v^2)}\left\{\frac{\partial}{\partial u}\left[(u^2+1)\frac{\partial\Phi}{\partial u}\right] + \frac{\partial}{\partial v}\left[(1-v^2)\frac{\partial\Phi}{\partial v}\right]\right\} + \frac{1}{c^2(u^2+1)(1-v^2)}\frac{\partial^2\Phi}{\partial\varphi^2} = 0. \tag{5}$$

Here $u=\sinh(\xi)$ and $v=\cos(\theta)$ with $\xi>0$ and $\theta\in[0,\pi]$. The oblate-spheroidal coordinates (u,v,φ) are related to Cartesian coordinates by

$$x = c\sqrt{(u^2+1)(1-v^2)}\cos\varphi, \tag{6a}$$

$$y = c\sqrt{(u^2+1)(1-v^2)}\sin\varphi, \tag{6b}$$

$$z = cuv. \tag{6c}$$

The second term in Eq. (5) can be omitted due to the symmetry by the azimuthal angle φ. The time-dependent solution of Eq. (5) is

$$\phi_i(u,v,t) = F_i(t)uv, \; u \leqslant u_i \tag{7a}$$

$$\phi_m(u,v,t) = v\{F_m(t)u + G_m(t)[u\cot^{-1}(u) - 1]\}, \quad u_i < u < u_o, \tag{7b}$$

$$\phi_o(u,v,t) = v\{-cE_o(t)u + G_o(t)[u\cot^{-1}(u) - 1]\}, \quad u > u_o. \tag{7c}$$

Here for an oblate spheroid $u_i=b_i/c$, $u_o=b_o/c$. Also, $F_i(t)$, $F_m(t)$, $G_m(t)$, and $G_o(t)$ are the coefficients that can be determined by proper boundary conditions at the interfaces of the three regions.

The Laplace (rather than the Poisson) equation has been used based on the assumption that charge inequalities arising from ionic transport during the electroporation process can be ignored on the ultrashort time scales. The current flows are not very large and so charge transfer during the ultrashort time scales ($\sim$ nanoseconds) of interest here, are indeed minimal. Invoking continuity in the potential and current density then leads to the following boundary conditions that are time dependent with variable conductivities and permittivities at the membrane:

$$\phi_o(u,v,t)|_{u_o} = \phi_m(u,v,t)|_{u_o}, \tag{8a}$$

$$\phi_m(u,v,t)|_{u_i} = \phi_i(u,v,t)|_{u_i}, \tag{8b}$$

$$\sigma_o E_u^o(t) + \varepsilon_o\frac{\partial E_u^o(t)}{\partial t}\bigg|_{u_o} = \sigma_m(t)E_u^m(t) + \varepsilon_m(t)\frac{\partial E_u^m(t)}{\partial t}\bigg|_{u_o}, \tag{8c}$$

$$\sigma_m(t)E_u^m(t) + \varepsilon_m(t)\frac{\partial E_u^m(t)}{\partial t}\bigg|_{u_i} = \sigma_i E_u^i(t) + \varepsilon_i\frac{\partial E_u^i(t)}{\partial t}\bigg|_{u_i}. \tag{8d}$$

Here $E_u=-\partial\phi/\partial u$ is the electric field along the u direction. Due to the membrane electroporation process, the parameters $\sigma_m(t)$ and $\varepsilon_m(t)$ become time dependent. These can be evaluated by the dynamic pore model, which combines Eqs. (4a)–(4c) and (7a)–(7c) with Eqs. (8a)–(8d). Then, all of the unknown coefficients $A_i(t)$, $A_m(t)$, $B_m(t)$, and $B_o(t)$ for the prolate spheroid case or $F_i(t)$, $F_m(t)$, $G_m(t)$, and $G_o(t)$ for the oblate spheroid case can be determined as discussed in the next section. Thus, the transmembrane potential is given as

$$\Delta\Phi = \phi_m(u_i,v,t) - \phi_m(u_o,v,t). \tag{9}$$

B. Dynamic pore model

Predictions of pore generation, growth and size evolution required for accurately characterizing membrane electroporation are based here on the continuum Smoluchowski theory. The following governing equation for the pore density distribution function $n(r,t)$ results [3–5,25–27,29], with r being the pore radius:

$$\frac{\partial n(r,t)}{\partial t} - \frac{D}{k_BT}\frac{\partial[n(r,t)\partial E(r)/\partial r]}{\partial r} - D\frac{\partial^2 n(r,t)}{\partial r^2} = S(r), \tag{10}$$

where $S(r)$ is the source or pore formation term and D is a pore diffusion constant. Physically, the diffusion process rep-

resents a "random walk" of the pore radius in "r space," brought about by fluctuations in radius arising from the constant entry and egress of water molecules and other species. The formation of pores is generally assumed to be a two-step process [26,36,70,71]. These reports assume pores to be initially created as hydrophobic and nonconducting, at a rate $S(r)$ per unit area of the membrane, during every time interval "dt." This rate is given as

$$S(r) = \frac{v_c h}{k_B T} \frac{dE(r)}{dr} \exp[-E(r)/(k_B T)]dr, \tag{11}$$

where v_c is an attempt rate density [72], $E(r)$ the energy for hydrophobic pores, T the operating temperature, and k_B the Boltzmann constant. If a nonconducting pore is created with a radius $r > r^*$ (=0.5 nm), it spontaneously changes its configuration and transforms into a conducting, hydrophilic pore. All conducting pores then survive as long as their radii remain larger than r^*. Destruction of a conducting pore occurs only if it drifts or diffuses in r space to a value below r^*. Due to the exponential term in Eq. (10), most pores are created with very small radii.

As shown in Eqs. (10) and (11), the energy $E(r)$ is the most important entity that governs the pore formation, growth and decay. This energy $E(r)$, which is a function of the pore radius "r," determines the "drift flux" for pores in r space [the left side of Eq. (10)], and the formation rate through Eq. (11). This energy function depends on several factors, including the membrane tension, the applied E field and associated stored electrostatic energy, and steric repulsion. These changes make $E(r)$ self-adjusting in response to pore formation, without causing uncontrolled growth and expansion. Thus, one has [48]

$$E(r) = 2\pi\gamma r - \int_0^r 2\pi\Gamma_{\text{eff}} A_p(r^*,t) r^* dr^* + (C/r)^4 - \pi\frac{\varepsilon_W - \varepsilon_m}{h} V^2 \int_0^r \alpha^2(r'') r'' dr'', \tag{12}$$

for a flat membrane, with $A_p(r,t)$ being the dynamic pore area, Γ_{eff} a variable membrane tension, and α a pore-dependent factor. Expressions of the tension Γ_{eff} and $A_p(r,t)$ are [48]

$$\Gamma_{\text{eff}}(A_p) = \Gamma_{\text{eff}}(A_p = 0) \frac{1 - [A_0/(A - A_p)]^2}{1 - (A_0/A)^2}, \tag{13a}$$

$$A_p(r,t) \approx A_0 \left(\int_0^r 2\pi r'' n(r'',t) dr'' \right). \tag{13b}$$

Here A_0 is the equilibrium area corresponding to minimum total interfacial energy. Area A slightly exceeds the equilibrium level A_0 and roughly, $A/A_0 = 1.0125$ yielding a tension of 10^{-3} J m^{-2} [48]. The pore area $A_p(r,t)$ dependent surface tension can become quite important for situations involving transient voltage pulses. In such cases, the voltage could fall to zero quickly (i.e., ultrashort ns pulses), thereby canceling out the electrostatic contribution to $E(r)$. However, the $A_p(r,t)$ term would continue to affect dynamical evolution over much longer periods.

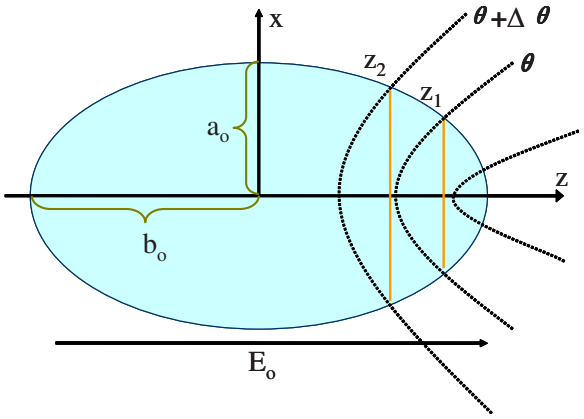

FIG. 2. (Color online) Schematic of the prolate spheroidal cell model for the surface area calculation of each segment.

Since the external electrical field is on the direction of the major axis of the prolate spheroidal cell, and the cell has rotational symmetry on φ direction, the whole cell can be discretized along the Z direction according to different θ as shown in Fig. 2. Here θ and the prolate spheroidal coordinate v has the following relationship: $v = \cos(\theta)$. Thus, from Eq. (2c), the Cartesian coordinate z can be expressed as $z = cuv = cu\cos(\theta)$. The surface area of each segment on the prolate spheroid is calculated by rotating the Cartesian ellipse $x^2/a_o^2 + z^2/b_o^2 = 1$ about its major axis as shown in Fig. 2. By the method of calculating the area of surface of revolution, we can obtain

$$A_0(\theta) = 2\pi \int_{p_2}^{p_1} \frac{ab^2}{c} \sqrt{1 - p^2} dp = \pi \frac{ab^2}{c} (p\sqrt{1 - p^2} + \arcsin p)\Big|_{p_2}^{p_1} = \pi \frac{ab^2}{c} [(p_1\sqrt{1 - p_1^2} + \arcsin p_1) - (p_2\sqrt{1 - p_2^2} + \arcsin p_2)]. \tag{14a}$$

In the above, $p_1 = e^2 u_o \cos(\theta)$, $p_2 = e^2 u_o \cos(\theta + \Delta\theta)$, and $e = c/b_o$ is the eccentricity of the prolate spheroid.

Similarly, the surface area of each segment from an oblate spheroidal cell is

$$A_0(\theta) = \pi \frac{ab^2}{c} [p_1\sqrt{1 + p_1^2} + \ln(p_1 + \sqrt{1 + p_1^2}) - p_2\sqrt{1 + p_2^2} + \ln(p_2 + \sqrt{1 + p_2^2})]. \tag{14b}$$

Here $p_1 = \frac{c^2}{b^2} u_o \cos(\theta)$ and $p_2 = \frac{c^2}{b^2} u_o \cos(\theta + \Delta\theta)$.

III. RESULTS AND DISCUSSION

Coupling Laplace's equations with the Smoluchowski equations yields the time-dependent transmembrane potential (TMP) across spheroidal cells. The electroporation-related time-dependent conductivity and permittivity changes at the membrane will eventually affect the TMP as shown in Fig. 3. This simulation result shown was obtained by considering a

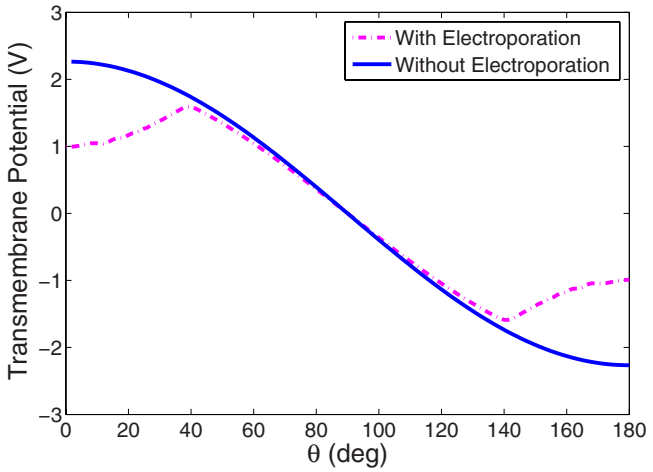

FIG. 3. (Color online) TMP versus angle (φ) for oblate spheroidal cells with minor-to-major axes ratio $a:b=3:1$. A 80 kV/cm, trapezoidal external pulse (with rise, fall, and on times of 0.5, 0.5, and 2 ns, respectively) was used for these simulations. The results shown are at $t=2.5$ ns.

simple one-shell oblate spheroidal model with a polar radius $b=5$ μm and equatorial radius $a=15$ μm. The membrane thickness was taken to be 5 nm at the polar points. The cell parameters used are given in Table I and are typical of biological cells. Most values were chosen from a study by Ermolina *et al.* [73]. The response of a high intensity 2 ns trapezoidal external pulse with $E=80$ kV/cm (0.5 ns rise and fall times), with time-dependent membrane conductivity (electroporation considered), was compared with identical cells having constant membrane conductivity. Figure 3 shows that the TMPs at polar points of the oblate cell ($a:b=3:1$) with electroporation, have much lower values than without electroporation. This is due to the formation of conducting pores on membrane, which results in the increase of conductivity at the polar points from an initial 5.3×10^{-6} S/m value to about 5.8×10^{-2} S/m. The higher conductivity due to electroporation at the poles reduces the voltage drop and pushes the peak TMP location to larger angular values. This feature is qualitatively similar to that reported for spherical cells [9].

A. Case for various geometries

Permeabilization is not only a function of electric field intensity and cell size but also of cell shape. To probe this further, comparative simulation were carried out for (i) a prolate spheroid with $a:b=1:3$ and polar radius $b=15$ μm, (ii) a spherical cell with radius $r=5$ μm, and (iii) an oblate spheroid with $a:b=3:1$ and $b=5$ μm. The same pulse used in Fig. 3 was applied for these simulations. The temporal development of TMP across spheroidal cells at $\theta=0°$ with different minor-to-major axes ($a:b$) ratios is shown in Fig. 4(a). Since the TMPs of spherical and prolate cells were lower than 1 V, no poration (as evaluated through the Smoluchowski equation), was predicted for these two cases. The peak TMP of oblate spheroidal cell is predicted to be about three times that of the spherical cell, and exceeds 1 V. The latter point perhaps requires some discussion, since traditionally this 1-V voltage has been accepted as the threshold for electroporation. For the traditional (long-duration) electroporative pulses, TMP does not really exceed this 1-V value since poration would set in at this level, thereby driving the local conductivities to high values and reducing the trans-membrane voltage drop. However, in the present case of ultrashort pulses, it becomes possible to exceed the 1-V magnitude during transient periods, leading to a "voltage overshoot." Physically, this occurs since a finite time and energy is required to rearrange the molecular structure within the membrane, and form conductive channels. Hence, excessive voltages beyond the customary 1-V threshold can be attained over ultrashort time durations, and do not necessarily cause irreversible damage [37]. In other words, despite the higher TMP, the molecules have not necessarily had the time to rearrange and form membrane pores.

TABLE I. Parameters used in simulations.

Conductivities (s/m):	
Cell membrane	5.3×10^{-6}
Cytoplasm	0.13
Environment	0.6
Dielectric Constant:	
Cell membrane	8.0
Cytoplasm	60.0
Environment	80.0

The TMP of oblate spheroidal cell in Fig. 4(a) decays rapidly after it reaches its maximum, even though the external pulse is on. This decrease occurs due to the TMP-controlled pore generation. The overall "voltage overshoot" behavior agrees well with a previous report on the time dependent behavior of the membrane voltage [74] on giant planar lipid membranes. As the external electric field is turned off beyond 3 ns, the transmembrane potentials converge to zero quickly with a time constant in the nanosecond range for the oblate case but rather larger ones for spherical and prolate spheroidal cells. This is the result of discharging of the membrane, which acts as a "leaky capacitor." For the oblate spheroid, a slight negative TMP value is predicted (brought about by the negative displacement current) at the end of the external pulse.

In order to better gauge the transmembrane potential profiles of different geometries, the TMPs versus polar angle (θ') are shown in Fig. 4(b) in spherical coordinates for the prolate, spherical, and oblate cases. A conversion between the polar angle (θ) in prolate spheroidal coordinates and polar angle (θ') in spherical coordinates can be realized by

$$\theta' = \cos^{-1}\left(\frac{z}{\sqrt{x^2+z^2}}\right) = \cos^{-1}\left(\frac{u\cos\theta}{\sqrt{u^2-1+\cos^2\theta}}\right). \tag{15a}$$

Similarly, the relationship between polar angle (θ) in spheroidal coordinates and polar angle (θ') in oblate spherical coordinates is

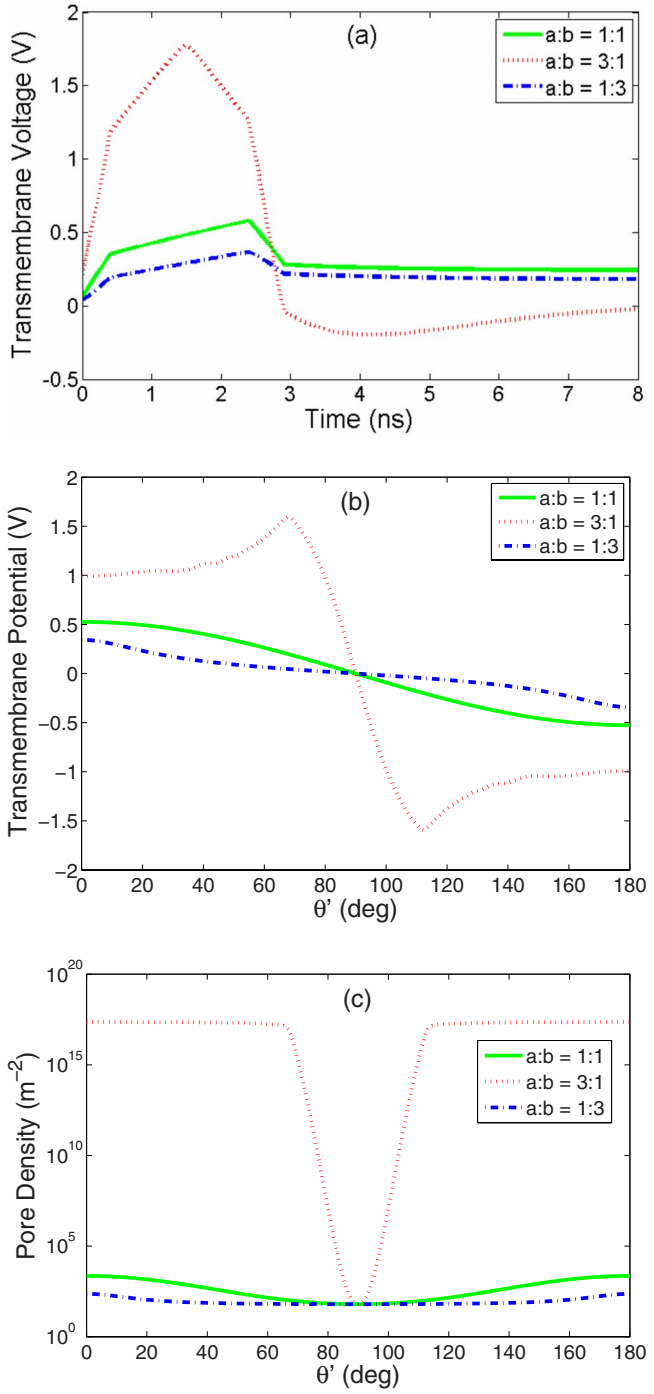

FIG. 4. (Color online) Simulation results for $a:b=1:3$ (prolate), 1:1 (spherical), and the 3:1 (oblate) cases. A 80 kV/cm, trapezoidal external pulse with and rise, fall, and on times of 0.5, 0.5, and 2 ns, respectively, was used for these simulations. (a) Results of the TMP versus time at $\theta=0°$. (b) Results of the TMP versus polar angle (θ) in spherical coordinates at $t=2.5$ ns. (c) Corresponding semilogarithmic plot of pore density versus polar angle (θ).

$$\theta' = \cos^{-1}\left(\frac{u\cos\theta}{\sqrt{u^2+1-\cos^2\theta}}\right). \tag{15b}$$

The results in Fig. 4(b) show that the shape of a spheroid determines the fraction of the membrane that is electroporated. Oblate spheroidal cell has much higher build-up TMP and is more prone to be electroporated than prolate and spherical ones. Physically, its shape is such that a larger and flatter surface area is "threaded" by the external electric field at the "poles" and the nearby regions. By comparison, the "poles" of the prolate spheroid where the electric field is the highest, presents a much sharper curvature. Hence, a smaller surface area experiences the same field magnitude as an oblate spheroid. One can thus expect stronger poration in oblate spheroidal geometries (with field parallel to the axis of symmetry) than in prolate spheroids or spheres. Also, the pores would cover a larger fraction of the surface area. This is borne out from calculations of the Smoluchowski equation (10) for the membrane pore density. The relationship between pore density and polar angle (θ') at $t=2.5$ ns for the three cases is shown in Fig. 4(c). About 78% of the membrane is electroporated with pore density in the order of 10^{17} per m^2. Pore densities for prolate spheroidal and spherical cases are very small, about 10^3 per m^2.

For oblate spheroidal cells, the TMP is strongly related to the flattening factor f, which is defined as $1-b/a$. Simulation results for oblate spheroidal cells with flattening $f=0.5, 0.65$, and 0.7 are shown in Fig. 5. A 65 kV/cm, trapezoidal external pulse with and rise, fall, and on times of 0.5, 0.5, and 2 ns, respectively, was used for these simulations. The results are measured at $t=3$ ns (when the pulse was off). Figure 5(a) shows that as flattening f increases, the cell membrane is more prone to be electroporated. With $f=0.5$, no field-induced conducting pores were predicted since the TMP is lower than 1 V. A small portion of membrane was electroporated when f was increased to 0.65. However, a little more than 2/3 of the membrane was electroporated when f was increased to 0.7. The semilogarithmic plot of pore density versus polar angle (θ') at $t=3$ ns for the three cases is shown in Fig. 5(b).

B. Cellular responses to different electrical pulses

As already discussed, the prolate cells are more difficult to electroporate than oblate spheroids. Thus, pulses with much higher intensities and long durations were used here to probe such effects in prolate cells. Simulation results shown in this section were obtained for a prolate cell with $b=25$ nm and $a:b=1:5$. First, a 200 kV/cm trapezoidal pulse with rise, fall, and on times of 1.5, 1.5, and 10 ns, respectively, was used across a prolate spheroidal cell. Figure 6 shows simulation results of the time-dependent TMP with cell properties as given in Table I. Three different times at 0.75 ns (middle of rise), 6.5 ns (middle of the pulse on-time), and 12.27 ns (middle of the fall time) were chosen to probe the angular dependence (θ) of the TMP. Obviously, no electroporation occurs at 0.75 ns since the pulse magnitude at this instant is still too small and the elapsed time too short. At 6.5 ns, the membrane for angles $\theta<50°$ is predicted to be electroporated with appreciable TMP decreases associated with the large local increments in membrane conductivity. However, the membrane voltage at the polar region is still predicted to be at (or above) 0.5 V. This is simply due to the relatively small size of the induced pores (not shown here)

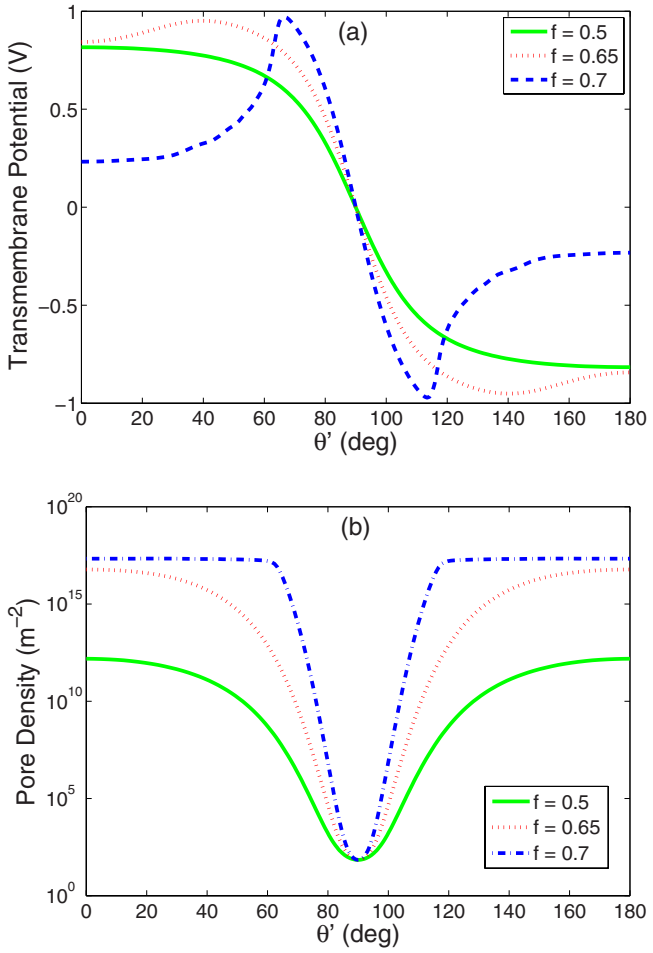

FIG. 5. (Color online) Simulation results for oblate spheroidal cells with flattening $f=0.5$, 0.65, and 0.7. A 65 kV/cm, trapezoidal external pulse with and rise, fall, and on times of 0.5, 0.5, and 2 ns, respectively, was used for these simulations. The results are measured at $t=3$ ns (when the pulse is off). (a) Results of the TMP versus polar angle (θ'). (b) Semilogarithmic plot of pore density versus polar angle (θ').

due to the ultrashort times, which restrict the magnitude of the external energy deposited. Consequently, the local membrane conductivity is not excessively large, and so the TMP dos not collapse to very small values. At 12.27 ns (middle of the pulse fall-time), the TMP at small angles θ in Fig. 6 is seen to be close to zero. This is the result of larger pore sizes and their higher density at these longer times. Also as expected, the TMP exhibits angular symmetry.

Results for the prolate spheroidal cell using the above conditions are alternatively shown as a function of time at specific angles in Fig. 7. Angular locations of $\theta=0°, 15°, 30°, 45°, 60°, 75°$, and 90° were selected. The temporal responses at the various angles are roughly the same. Voltage overshoots occur with delays that increase progressively with the angle. Furthermore, for the $\theta=0°, 15°$, and 30° locations, the TMPs tend to decay to zero soon after the external pulse is turned off. But for $\theta=45°, 60°, 75°$, the TMPs take relatively longer time for discharging. This is due to the lower membrane pore density (and hence, conductance) that effectively increases the "distributed RC" time constant. At $\theta=90°$, the TMP is always zero since the membrane is perpendicular to the external electrical field.

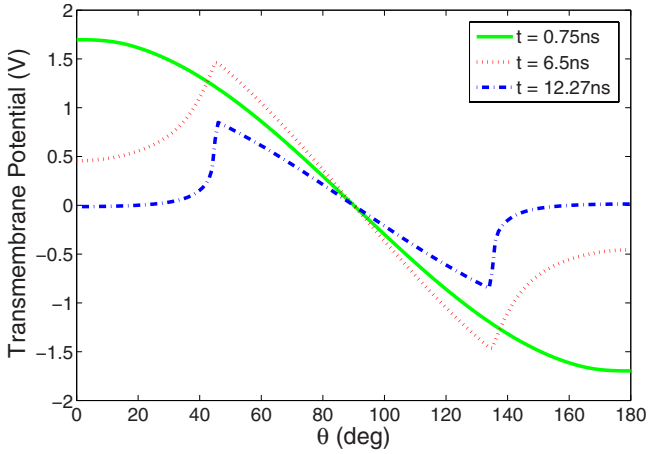

FIG. 6. (Color online) TMP versus θ for a prolate spheroidal cell ($a:b=1:5$) at three different times of 0.75 ns (middle of pulse rise), 6.5 ns (middle of pulse-on time), and 12.25 ns (middle of pulse fall). A 200 kV/cm, trapezoidal external pulse with rise, fall, and on times of 1.5, 1.5, and 10 ns, respectively, was used for these simulations.

The relationship between different pulse intensities and TMP was studied next. Figure 8 shows the TMPs for prolate spheroid ($a:b=1:5$) under pulses with the same pulse duration $t_{on}=10$ ns but with different field intensities ($E=100, 150, 200$, and 250 kV/cm). The rise, fall, and on times of the external pulse were taken to be 1.5, 1.5, and 10 ns, respectively. A snapshot at 11.5 ns (just prior to pulse fall-off) for the TMP versus θ in each case, is shown in Fig. 8(a). The TMP curve corresponding to $E=100$ kV/cm shows no electroporation on the cellular membrane since the pulse duration is too small. The polar points bear the highest TMP across the whole membrane while the equatorial points have

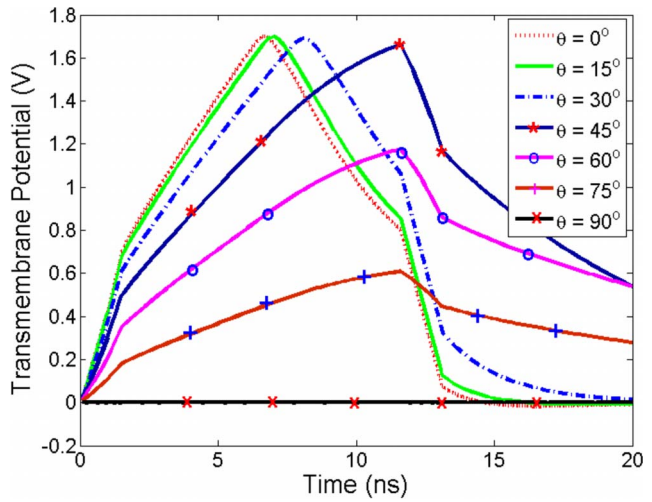

FIG. 7. (Color online) TMP versus time for a prolate spheroidal cell ($a:b=1:5$) at the different angular locations of $\theta=0°$, 15°, 30°, 45°, 60°, 75°, and 90°. Here the polar radius $b=25$ μm. The trapezoidal external pulse used was the same as in Fig. 6.

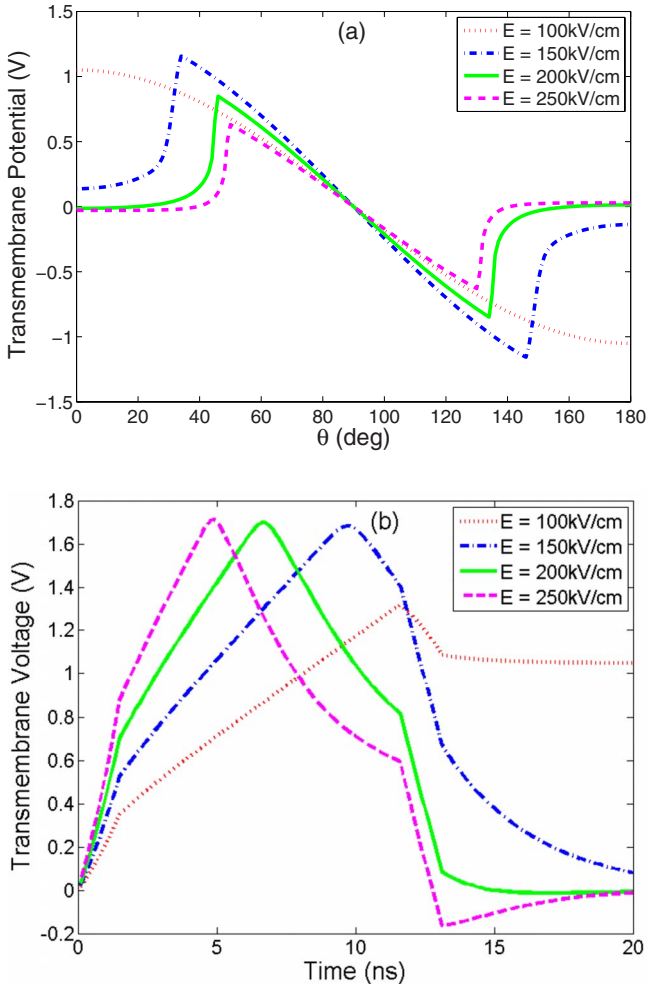

FIG. 8. (Color online) A prolate spheroid ($a:b=1:5$) cell under applied pulses with 10 ns duration but with different intensities ($E=100$, 150, 200, and 250 kV/cm). The rise and fall times of the external pulse were taken to be 1.5 ns. (a) A 11.5 ns snapshot of TMP versus θ and (b) TMP versus time at the $\theta=0°$ location.

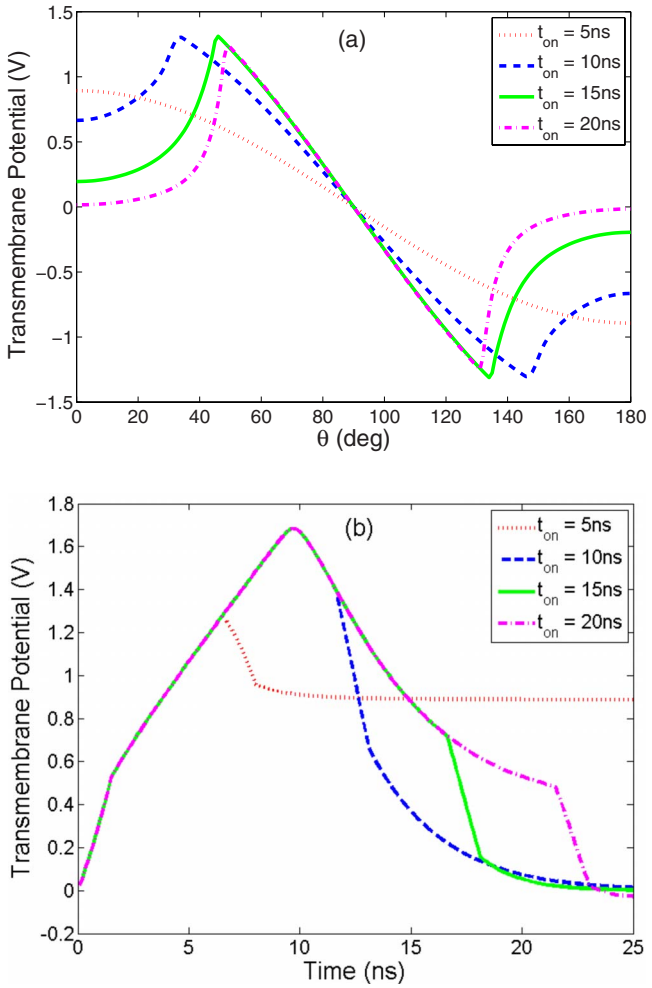

FIG. 9. (Color online) A prolate spheroid ($a:b=1:5$) cell under pulses with the same intensity $E=150$ kV/cm but with different on times ($t_{on}=5$, 10, 15, and 20 ns, respectively). (a) TMP versus θ at the end of each pulse. (b) TMP versus time at $\theta=0°$.

zero TMP. With electrical field intensities increasing from 150–250 kV/cm, the fractions of the electroplated membrane increase from 39 to 56 %. The TMPs of $E=250$ kV/cm has the lowest value among the four cases because the pore density and size are the largest. This results in the lowest membrane conductivity. Figure 8(b) shows temporal development of the TMP for a prolate spheroidal cell at the $\theta=0°$ location for various pulse intensities. The results show that for $E=100$ kV/cm, the intact membrane would have the longest discharge time, while in the remaining three cases the membrane voltage recovers back to zero over subnanosecond time frames.

The relationship between different pulse durations and TMP for prolate spheroidal cell is shown in Fig. 9. The TMPs for the prolate spheroid cell subjected to external pulses with the same intensity $E=150$ kV/cm but different pulse durations ($t_{on}=5$, 10, 15, and 20 ns, respectively) were used. The rise and fall times of the external pulse were both taken to be 1.5 ns. Figure 9(a) shows the TMP versus θ at the end of each pulse, while Fig. 9(b) shows the temporal development of TMP at polar points. The predictions in Fig. 9(a) are for the membrane to remain intact with the 5 ns pulse, but to get 33–50 % electroporated for pulses of 10 ns or longer. Figure 9(b) shows that at $\theta=0$, except for $t_{on}=5$ ns, the TMPs of the remaining three cases (i.e., $t_{on}=10$, 15, and 20 ns) show relatively similar behavior. The recovery time constant is expectedly lower for the higher duration pulses due to their larger porative (and hence conductivity modulation) effects.

For completeness, the relationship between the TMP versus the polar angle θ for prolate and oblate spheroidal cells at different electric-field orientation angles "α" is shown in Fig. 10. The rise, fall, and on times of the trapezoidal external pulse were 1.5, 1.5, and 10 ns, respectively, with $E_0=50$ kV/cm. Values of $\alpha=0°$, 30°, 45°, 60°, and 90° were chosen. Figure 10(a) shows the angular variation for the prolate spheroidal case with $a:b=3$ μm:5 μm. When $\alpha=0°$, the TMP has its lowest peak value at $\theta=0°$, since the field is along the z direction where the spheroidal cell has minimum curvature. For the other three cases of $\alpha=30°$, 45°, and 60°, the TMP peak values increase as α increases. However, the peak occurs at polar angles θ of 50°, 65°, and 75°, respectively, which are greater than the corresponding α values.

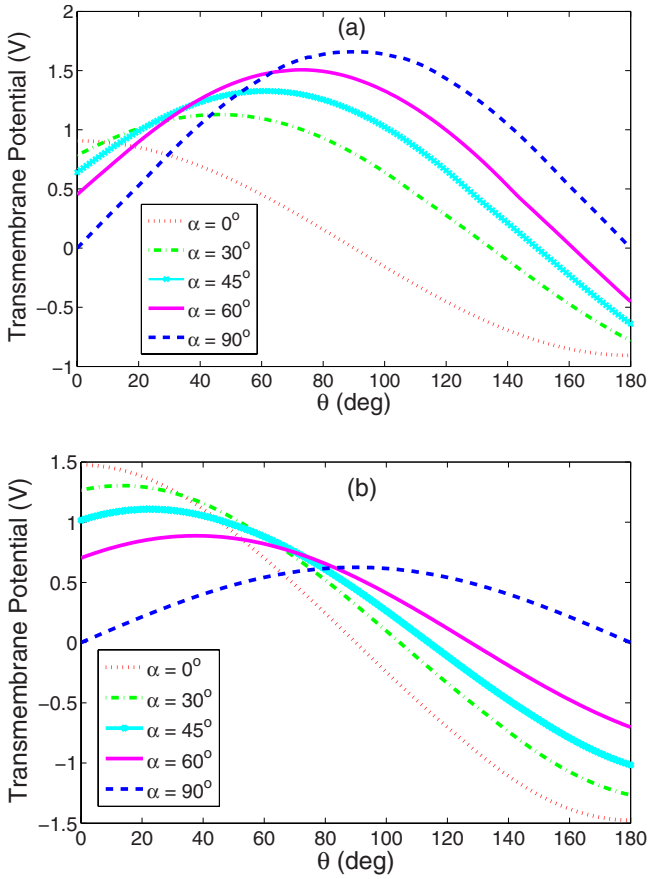

FIG. 10. (Color online) Total outer membrane TMP versus the polar angle θ at $t=11.5$ ns for prolate ($a:b=3\mu$m$:5$ μm) and oblate ($a:b=5\mu$m$:3$ μm) spheroidal cells under a 50 kV/cm external E field. Angular field orientations of $\alpha=0°$, 30°, 45°, 60°, and 90° were used. (a) Prolate spheroidal case and (b) the oblate spheroidal case.

This is due to the dominance of the E_x induced TMP over that induced by E_z. Figure 10(b) shows TMPs for an oblate spheroidal cell ($a:b=5$ μm$:3$ μm). Unlike the prolate spheroidal case, the TMP has the highest peak value at $\theta=0°$ when $\alpha=0°$, and the lowest peak value at $\theta=90°$ when $\alpha=90°$. This is to be expected, since the flattest surface for the oblate spheroid occurs at $\alpha=0°$ rather than $\alpha=90°$. For the cases with $\alpha=30°$, 45°, and 60°, the TMP peak values decrease as α increases.

Finally, results probing the size effects on the TMP are given in Fig. 11. Cells with two different semimajor axis lengths, but the same aspect ratio were used. The total TMP versus polar angle θ at an angular field orientation of $\alpha=15°$ for two prolate spheroids with the same aspect ratio ($a:b=1:5$) but different lengths ($a=1$ μm, 5 μm) were considered. A 50 kV/cm, trapezoidal external pulse with rise, fall, and on times of 1.5, 1.5, and 10 ns, respectively, was used for these simulations. A relatively modest field was chosen to avoid electroporation effects and maintain a relatively simpler situation. As seen from Fig. 11, the larger cell develops a slightly higher TMP. This is qualitatively in keeping with the trend seen in spherical cells. However, the TMP ratio between the two is substantially different from the 1:5 ratio of their axes.

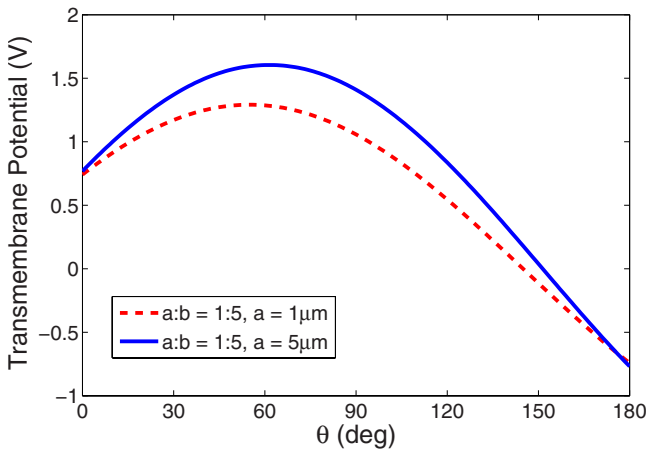

FIG. 11. (Color online) Total TMP versus the polar angle θ at angular field orientation of $\alpha=15°$ for two prolate spheroids having the same aspect ratio ($a:b=1:5$) but different axis lengths $a=1$ μm and $a=5$ μm. A 50 kV/cm, trapezoidal external pulse with rise, fall, and on times of 1.5, 1.5, and 10 ns, respectively, was used for these simulations.

IV. SUMMARY AND CONCLUSIONS

In summary, self-consistent evaluations of both the transmembrane potential and possible electroporation density across membrane of spheroidal cells in response to ultrashort, high-intensity pulses have been reported and discussed. Most treatments in the literature on this subject have been assumed spherical cells. However, in biology, examples of such spherical shapes are rare, though many of the cells deviating from the spherical shape do exhibit rotational symmetry. For this reason, spheroidal cells were chosen as the logical first step. Though a few treatments of spheroidal cells have recently been reported [63–66], the poration aspect and its role in self-consistently modifying the TMP, including its angular dependence, had been taken into account. The present study coupled the Laplace equation with Smoluchowski theory of pore formation, to yield dynamic membrane conductivities that influence the TMP. It may be mentioned though, that the present study was restricted to single-shell models, with the focus being on the plasma membrane. Extensions to double-shell models are underway, and comprehensive results will be reported elsewhere.

It has been shown here that the TMP induced by pulsed external voltages can be substantially higher in oblate spheroids, in comparison to both spherical and prolate spheroidal cells. Flattening of the surface area in oblate spheroids leads to both higher electric fields seen by the membrane, and allows a great fraction of the surface area to be porated. From a practical standpoint, this suggests that drug-delivery and molecular or ionic uptake that is the basis for electrochemotherapy, could work best for flatter-shaped cells. In addition, external fields could be applied to orient the cells for optimal uptake based on field interactions with the induced dielectric moment [75]. For example, based on energy minimization considerations, spheroids can be oriented either parallel or perpendicular to their symmetry axis by ac fields depending on the applied frequency [76]. Results have also

been obtained with electric field at arbitrary angular orientation to the semimajor axis. Finally, by probing cells with the same shape but widely different sizes, a strong departure from simple scaling of the TMP with dimension has been shown.

The trends obtained are general, and the theory would apply to periodic (e.g., harmonic) excitations from an external source as well. The charging time constant of the plasma membrane would then be expected to be in the microsecond regime, with the maximum voltage in oblate spheroids being larger than in spherical or prolate cells. For arbitrary orientations of the external field with respect to the major axis of the spheroid, relative differences in the TMP, pore density and formation times between the different shapes would be expected to reduce somewhat.

ACKNOWLEDGMENTS

The authors thank Professor K. H. Schoenbach (Old Dominion University) and Professor D. Miklavcic (University of Ljubljana) and for useful discussions. Partial support from Central Michigan University is also gratefully acknowledged.

[1] J. Teissié, N. Eynard, B. Gabriel, and M. P. Rols, Adv. Drug Delivery Rev. **35**, 3 (1999).
[2] J. R. Beveridge, S. J. MacGregor, L. Marsili, J. G. Anderson, N. J. Rowan, and O. Farish, IEEE Trans. Plasma Sci. **30**, 1525 (2002).
[3] E. Neumann, A. E. Sowers, and C. A. Jordan, *Electroporation and Electrofusion in Cell Biology* (Plenum, New York, 1989).
[4] T. Y. Tsong, Biophys. J. **60**, 297 (1991).
[5] D. C. Chang, B. M. Chassy, J. A. Saunders, and A. E. Sowers, *Guide to Electroporation and Electrofusion* (Academic, San Diego, 1992).
[6] L. M. Mir, L. F. Glass, G. Sersa, J. Teissie, C. Domenge, D. Miklavcic, M. J. Jaroszeski, S. Orlowski, D. S. Reintgen, Z. Rudolf, M. Belehradek, R. Gilbert, M. P. Rols, J. Belehradek, Jr., J. M. Bachaud, R. Conti, B. Stabuc, M. Cemazar, P. Coninx, and R. Heller, Br. J. Cancer **77**, 2336 (1998).
[7] E. Neumann, K. Toensing, S. Kakorin, P. Budde, and J. Frey, Biophys. J. **74**, 98 (1998).
[8] A. Gothelf, L. M. Mir, and J. Gehl, Cancer Treat Rev. **29**, 371 (2003).
[9] K. C. Smith, J. C. Neu, and W. Krassowska, Biophys. J. **86**, 2813 (2004).
[10] U. Zimmermann and G. A. Neil, *Electromanipulation of Cells* (CRC Press, Boca Raton, FL, 1996).
[11] G. Sersa, D. Miklavci, M. Cemazar, Z. Rudolf, G. Pucihar, and M. Snoj, Eur. J. Surg. Oncol. **34**, 232 (2008).
[12] G. Pucihar, L. M. Mir, and D. Miklavcic, Bioelectrochemistry **57**, 167 (2002).
[13] L. H. Li, M. L. Hensen, Y. L. Zhao, and S. W. Hui, Biophys. J. **71**, 479 (1996).
[14] M. F. Kalady, M. W. Onaitis, K. M. Padilla, S. Emani, D. S. Tyler, and S. K. Pruitt, Surg. Forum **52**, 225 (2001).
[15] E. Eksioglu-Demiralp, S. Kitada, D. Carson, J. Garland, A. Andreef, and J. C. Reed, J. Immunol. Methods **275**, 41 (2003).
[16] H. Mekid and L. M. Mir, Biochim. Biophys. Acta **1524**, 118 (2001).
[17] C. Ramos and J. Teissie, Biochimie **82**, 511 (2000).
[18] R. Staempfli, An. Acad. Bras. Cienc. **30**, 57 (1958).
[19] E. Neumann and K. Rosenheck, J. Membr. Biol. **10**, 279 (1972).
[20] S. Somiari, J. Glasspool-Malone, J. J. Drabick, R. A. Gilbert, R. Heller, M. J. Jaroszeski, and R. W. Malone, Curr. Opin. Mol. Ther. **2**, 78 (2000).
[21] M. Golzio, L. Mazzolini, P. Moller, M. P. Rols, and J. Teissié, Gene Ther. **12**, 246 (2005).
[22] E. Lindahl, B. Hess, and D. van der Spoel, J. Mol. Model. **7**, 306 (2001).
[23] J. J. Lopez Cascales, J. Garcia de la Torre, S. J. Marrink, and H. J. C. Berendsen, J. Chem. Phys. **104**, 2713 (1996).
[24] D. P. Tieleman, H. Leontiadou, A. E. Mark, and S. J. Marrink, J. Am. Chem. Soc. **125**, 6382 (2003).
[25] V. F. Pastushenko, Yu A. Chhizmadzhev, and V. B. Arakelyan, Bioelectrochem. Bioenerg. **6**, 53 (1979).
[26] J. C. Neu and W. Krassowska, Phys. Rev. E **59**, 3471 (1999).
[27] J. C. Weaver, IEEE Trans. Plasma Sci. **28**, 24 (2000).
[28] A. Barnet and J. C. Weaver, Bioelectrochem. Bioenerg. **25**, 163 (1991).
[29] R. P. Joshi, Q. Hu, R. Aly, K. H. Schoenbach, and H. P. Hjalmarson, Phys. Rev. E **64**, 011913 (2001).
[30] K. C. Smith, T. R. Gowrishankar, A. T. Esser, D. A. Stewart, and J. C. Weaver, IEEE Trans. Plasma Sci. **34**, 1394 (2006).
[31] J. Teissie, M. Golzio, and M. P. Rols, Biochim. Biophys. Acta **1724**, 270 (2005).
[32] K. C. Melikov, V. A. Frolov, A. Shcherbakov, A. V. Samsonov, Y. A. Chizmadzhev, and L. V. Chernomordik, Biophys. J. **80**, 1829 (2001).
[33] K. H. Schoenbach, R. P. Joshi, J. Kolb, N. Chen, M. Stacey, P. Blackmore, E. S. Buescher, and S. J. Beebe, Proc. IEEE **92**, 1122 (2004).
[34] P. T. Vernier, Y. Sun, L. Marcu, S. Salemi, C. M. Craft, and M. A. Gundersen, Biochem. Biophys. Res. Commun. **310**, 286 (2003).
[35] S. J. Beebe, P. F. Blackmore, J. White, R. P. Joshi, and K. H. Schoenbach, Physiol. Meas **25**, 1077 (2004).
[36] K. H. Schoenbach, F. E. Peterkin, R. W. Alden, and S. J. Beebe, IEEE Trans. Plasma Sci. **25**, 284 (1997).
[37] K. H. Schoenbach, S. J. Beebe, and E. S. Buescher, Bioelectromagnetics (N.Y.) **22**, 440 (2001).
[38] R. P. Joshi, Q. Hu, R. Aly, K. H. Schoenbach, and H. P. Hjalmarson, Phys. Rev. E **64**, 011913 (2001).
[39] A. J. H. Sale and W. A. Hamilton, Biochim. Biophys. Acta **148**, 781 (1967); **163**, 37 (1968).
[40] K. H. Schoenbach, R. P. Joshi, R. H. Stark, F. C. Dobbs, and S. J. Beebe, IEEE Trans. Dielectr. Electr. Insul. **7**, 637 (2000).
[41] R. Nuccitelli, U. Pliquett, X. Chen, W. Ford, R. J. Swanson, S. J. Beebe, J. F. Kolb, and K. H. Schoenbach, Biochem. Bio-

phys. Res. Commun. **343**, 351 (2006).
[42] M. Stacey, J. Stickley, P. Fox, V. Statler, K. H. Schoenbach, S. J. Beebe, and S. Buescher, Mutat Res. **542**, 65 (2003).
[43] R. P. Joshi, A. Mishra, J. Song, A. Pakhomov, and K. H. Schoenbach, IEEE Trans. Biomed. Eng. **55**, 1391 (2008).
[44] R. P. Joshi, A. Mishra, Q. Hu, K. H. Schoenbach, and A. Pakhomov, Phys. Rev. E **75**, 061906 (2007).
[45] Z. Vasilkoski, A. T. Esser, T. R. Gowrishankar, and J. C. Weaver, Phys. Rev. E **74**, 021904 (2006).
[46] J. C. Neu and W. Krassowska, Phys. Rev. E **67**, 021915 (2003).
[47] R. P. Joshi, Q. Hu, and K. H. Schoenbach, IEEE Trans. Dielectr. Electr. Insul. **10**, 778 (2003).
[48] R. P. Joshi, Q. Hu, K. H. Schoenbach, and H. P. Hjalmarson, Phys. Rev. E **65**, 041920 (2002).
[49] Q. Hu, R. P. Joshi, and K. H. Schoenbach, Phys. Rev. E **72**, 031902 (2005).
[50] Q. Hu, S. Viswanadham, R. P. Joshi, K. H. Schoenbach, S. J. Beebe, and P. F. Blackmore, Phys. Rev. E **71**, 031914 (2005).
[51] P. T. Vernier, M. J. Ziegler, Y. Sun, W. V. Chang, M. A. Gundersen, and D. P. Tieleman, J. Am. Chem. Soc. **128**, 6288 (2006).
[52] A. G. Pakhomov, J. F. Kolb, J. A. White, R. P. Joshi, S. Xiao, and K. H. Schoenbach, Bio-Electromagn. J. **28**, 655 (2007).
[53] A. G. Pakhomov, A. Phinney, J. Ashmore, K. Walker, III, J. F. Kolb, S. Kono, K. H. Schoenbach, and M. R. Murphy, IEEE Trans. Plasma Sci. **32**, 1579 (2004).
[54] K. H. Schoenbach, S. Xiao, R. P. Joshi, J. T. Camp, T. Heeren, J. F. Kolb, and S. J. Beebe, IEEE Trans. Plasma Sci. **36**, 414 (2008).
[55] J. Gimsa and D. Wachner, Biophys. J. **77**, 1316 (1999).
[56] B. L. Batzing, *Microbiology: An Introduction* (Thompson Learning, Pacific Grove, CA, 2002).
[57] M. Radu, M. Ionescu, N. Irimescu, K. Iliescu, R. Pologea-Moraru, and E. Kovacs, Biophys. J. **89**, 3548 (2005).
[58] F. J. Asencor, C. Santamaria, F. J. Iglesias, and A. Dominguez, Biophys. J. **64**, 1626 (1993).
[59] G. Pucihar, T. Kotnik, B. Valic, and D. Miklavcic, Ann. Biomed. Eng. **34**, 642 (2006).
[60] M. Pavlin, N. Pavselj, and D. Miklavcic, IEEE Trans. Biomed. Eng. **49**, 605 (2002).
[61] T. R. Gowrishankar and J. C. Weaver, Proc. Natl. Acad. Sci. U.S.A. **100**, 3203 (2003).
[62] R. P. Joshi, A. Mishra, and K. H. Schoenbach, IEEE Trans. Plasma Sci. **36**, 1680 (2008).
[63] T. Kotnik and D. Miklavcic, Biophys. J. **79**, 670 (2000).
[64] K. Maswiwat, D. Wachner, R. Warnke, and J. Gimsa, J. Phys. D **40**, 914 (2007).
[65] J. Gimsa and D. Wachner, Eur. Biophys. J. **30**, 463 (2001).
[66] K. Waswiwat, D. Wachner, and J. Gimsa (unpublished).
[67] R. P. Joshi, Q. Hu, and K. H. Schoenbach, IEEE Trans. Plasma Sci. **32**, 1677 (2004).
[68] R. A. Jerry, A. S. Popel, and W. E. Brownell, IEEE Trans. Biomed. Eng. **43**, 970 (1996).
[69] M. Abramowitz and I. A. Stegun, in *Handbook of Mathematical Functions with Formulas, Graphs, and Mathematical Tables* (Dover, New York, 1972), p. 752.
[70] J. C. Weaver, Ann. N.Y. Acad. Sci. **720**, 141 (1994).
[71] J. Teissie and M. P. Rols, Ann. N.Y. Acad. Sci. **720**, 98 (1994).
[72] J. C. Weaver and R. A. Mintzer, Phys. Lett. **86A**, 57 (1981).
[73] I. Ermolina, Y. Polevaya, Y. Feldman, B. Ginzburg, and M. Schlesinger, IEEE Trans. Dielectr. Electr. Insul. **8**, 253 (2001).
[74] W. Meier, A. Graff, A. Diederich, and M. Winterhalter, Phys. Chem. Chem. Phys. **2**, 4559 (2000).
[75] J. Gimsa, Biochemistry **54**, 23 (2001).
[76] M. Saito, H. P. Schwan, and G. Schwarz, Biophys. J. **6**, 313 (1966).